



Electrochemical regeneration of columnar activated carbon saturated with acid orange 7

Heng Yuan, Wangfeng Cai, Ding Lu, Yan Wang*

School of Chemical Engineering and Technology, Tianjin University, Tianjin 300350, China, Tel. +86–13920533780; Fax: +86–022–23761975; email: zhuwangyan@tju.edu.cn (Y. Wang), Tel. +86–15822632765; email: lsnloveyh@tju.edu.cn (H. Yuan), Tel. +86–18602619853; email: Wfcai@tju.edu.cn (W. Cai), Tel. +86–18526283802; email: ludingde@tju.edu.cn (D. Lu)

Received 28 June 2018; Accepted 12 December 2018

ABSTRACT

We investigated the electrochemical regeneration of columnar activated carbon (CAC) saturated with acid orange 7 (AO7). The feasibility of the electrochemical regeneration was assessed in terms of regeneration efficiency as well as the structural properties and surface chemistry of the CAC before and after regeneration. The effects of electrolysis time, electrolyte concentration, applied current density, electrolysis treatment (either anodic or cathodic), and solution pH were systematically evaluated. Under the optimum conditions (current density of 22.86 mA cm^{-2} ; regeneration time of 6 h; cathodic electrolysis treatment; electrolyte concentration of $0.1 \text{ M Na}_2\text{SO}_4$; and solution pH of 11.5), a CAC regeneration efficiency of 81% was achieved. We also examined the kinetics, isotherms, and thermodynamic parameters for the adsorption of AO7 onto CAC before and after regeneration. Both sets of adsorption equilibrium data could be fitted using the Langmuir isotherm. However, the kinetics of AO7 adsorption onto CAC before and after regeneration were different. Upon regeneration, the predominant mechanism of the adsorption process changed from a reaction-controlled mechanism to a diffusion-controlled mechanism. Furthermore, the thermodynamic parameters (e.g. ΔG° , ΔH° , and ΔS°) for CAC were evaluated before and after regeneration, revealing that both adsorption processes were endothermic and spontaneous.

Keywords: Electrochemical regeneration; Acid orange 7; Activated carbon; Adsorption equilibrium; Adsorption kinetics; Thermodynamic parameters

1. Introduction

Many manufacturers, such as those in the textiles, dye-stuffs, paper, and plastics industries, use dyes to color their products. This generates a considerable amount of colored wastewater [1]. Furthermore, many of the dyes in colored wastewater are toxic and/or carcinogenic [2,3]. Therefore, it is necessary to lower dye concentrations in wastewater to the standards of national and international regulatory agencies before it is discharged into the environment [4]. Dyes can be effectively removed using adsorption. Activated carbon has been widely applied as an adsorbent in the treatment of industrial water effluents because of its high surface area, various pore structures, rich surface chemistry, and high

adsorption capacity [5–9]. However, pollutant-saturated activated carbon is often disposed of in landfills or incinerated, both of which waste carbon resources, introduce secondary pollutants into the environment, and increase the cost of adsorption operating processes [5,7,8,10]. Therefore, the reuse of exhausted activated carbon using effective regeneration approaches should be explored. Thermal regeneration is a high-efficiency process that is the most widely used in industrial applications [11]. However, it presents disadvantages in terms of high energy consumption, high cost, the need for ex situ operation, possible changes in the properties of the activated carbon, and considerable loss ($\approx 10\text{--}15\%$ by weight) during processing [11,12–14]. Another widely used method is chemical regeneration. This method is simple and

* Corresponding author.

inexpensive, but its efficiency is typically below 70%, and approximately 10–15% of the pores in the activated carbon remain blocked after treatment [11]. Moreover, the desorbed pollutants are not destroyed, necessitating expensive purification steps to recover the solvent [15].

Electrochemical regeneration of spent activated carbon has gained increasing research attention in recent years because it can be performed at low temperatures, additional chemicals are not required, organics deposited on the activated carbon can be cracked in situ without affecting the structural properties or characteristics of the activated carbon [16], and organic pollutants can be degraded to less hazardous compounds or completely mineralized [8,17].

Because of their chemical stability and thus resistance to biodegradation, azo dyes are among the largest group of colorants used in industry [18,19]. Acid orange 7 (AO7) is a widely used non-reactive acid azo dye [20]. Therefore, the aim of the current study was to investigate the electrochemical regeneration of commercial columnar activated carbon (CAC) saturated with AO7.

We conducted experiments to investigate the effects of electrolysis time, electrolyte concentration, applied current density, electrolysis treatment (either anodic or cathodic), and pH of the solution upon regeneration efficiency (RE). We also evaluated the structural properties and surface chemistry of the CAC before and after regeneration. Furthermore, to thoroughly investigate the changes in the CAC, adsorption experiments were performed to obtain the kinetics, isotherms, and thermodynamic parameters of AO7 adsorption on CAC before and after regeneration. Accordingly, it is hoped that the results of this study will provide useful information for the design of a CAC regeneration system.

2. Experimental setup

2.1. Materials

Commercial CAC (3–8 mm in length, Fujian Xinsen Carbon Industry Co., Ltd., China) was used as the adsorbent. Before saturation, the CAC samples were washed several times with distilled water and dried in air at 378 K for 24 h. AO7 (>85%, Macklin) and distilled water were used to prepare the aqueous solutions for the tests. The chemicals used in the electrolytes and for evaluating the acid-base properties were of analytical reagent grade and were obtained from Tianjin Kemiou Chemical Reagent Co., Ltd. (Tianjin, China).

2.2. Electrochemical regeneration reaction system

A schematic of the experimental setup is given in Fig. 1. It consists of a rectangular electrode chamber made from polymethyl methacrylate (0.04 m × 0.05 m × 0.10 m), a reservoir with an effective volume of 0.5 L, a peristaltic pump (model: YZ1515x, purchased from Longer Precision Pump Co., Ltd.) connecting the electrode chamber with the reservoir and a power supply (model: RXN-305D, Zhaoxin; purchased from Shenzhen Zhaoxinyuan Electronic Technology Co., Ltd.), with a capacity of 0–5 A/0–30 V. A micropore plate made of Teflon was fitted at the bottom of the electrode chamber to evenly distribute the electrolyte inside the electrode chamber. Two graphite plates, each with an active area

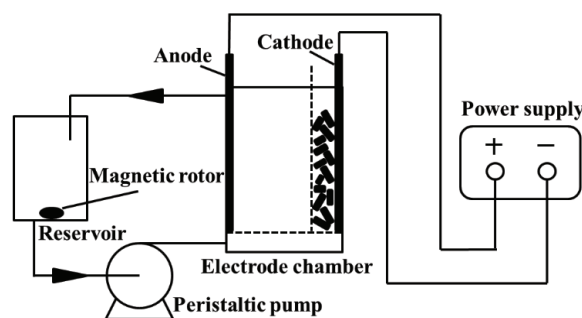


Fig. 1. Schematic of the experimental setup.

of 0.0035 m² (0.05 m × 0.07 m × 0.002 m), were used as the anode and cathode. The electrodes were fixed in the electrode chamber at an inter-electrode distance of 36 mm, and one side of the chamber was filled with spent CAC secured using a Teflon micropore plate. Two distinct experiments were carried out in the present investigation: (1) electrochemical regeneration of spent CAC, and (2) adsorption studies using fresh and regenerated CAC.

2.3. AO7 saturation of activated carbon

Adsorption data for the saturation of activated carbon were obtained from closed batch experiments. AO7 solutions (150 mL) with an initial concentration of 500 mg L⁻¹ were added to 250-mL glass flasks containing 0.5 g of virgin activated carbon. The flasks were sealed to avoid evaporation and placed on a shaker at a constant speed of 200 rpm (≈3.3 Hz) with a thermostatically controlled bath at 303 K for 72 h to attain equilibrium. After reaching equilibrium, the saturated activated carbon samples were dried in air at 378 K for 12 h.

2.4. Electrochemical regeneration of CAC

The electrochemical regeneration of activated carbon was carried out in the electrode chamber described in section 2.2. Prior to regeneration, 0.5 g of the AO7-saturated CAC was immersed in the electrolyte solution (250 mL) for 12 h to eliminate the influence of solvent extraction, placed into the chamber, and kept in close contact with either the anode (anodic regeneration experiments) or cathode (cathodic regeneration experiments) using a micropore plate made of Teflon. We chose sodium sulphate as the electrolytic solution rather than sodium chloride because the production of oxidized chlorine species can produce toxic chlorinated hydrocarbons [7,21,22]. The electrolyte solution (250 mL) was continuously stirred and recirculated through the reservoir and chamber at a speed of 1.29 mL s⁻¹ using a peristaltic pump. All experiments were conducted at room temperature and atmospheric pressure.

During the regeneration experiments, the concentration of AO7 was measured using UV-Vis absorption spectroscopy (Shimadzu UV-2550) at 485 nm after sampling, and the pH values of the electrolyte solutions were adjusted by adding 0.1 M NaOH or 0.1 M H₂SO₄. The pH was measured using a pH meter (model: PHSJ-4F, Shanghai INESA Scientific Instrument Co., Ltd.).

2.5. Adsorption kinetics

The kinetics of AO7 adsorption onto virgin columnar activated carbon (V-CAC) or CAC that had been previously regenerated columnar activated carbon (r-CAC) under optimum conditions were assessed using a thermostatted rotary shaker (200 rpm, ≈ 3.3 Hz) at 303, 313, or 323 K for 72 h. An AO7 solution (150 mL) with an initial concentration of 100, 300, or 500 mg L⁻¹ was added to a 250-mL glass flask containing 0.5 g of V-CAC or r-CAC. The flask was sealed to avoid evaporation, and small amounts of the sample were taken at regular intervals for the kinetic study.

2.6. Adsorption equilibrium isotherms

Adsorption equilibrium isotherms were obtained from closed-batch experiments. V-CAC or r-CAC (0.5 g) was added to a flask containing 150 mL of an AO7 solution with a concentration of 100, 150, 200, 250, 300, 400, or 500 mg L⁻¹. The sealed flask was shaken (200 rpm ≈ 3.3 Hz) at 303, 313, or 323 K for 72 h to reach equilibrium. After equilibrium, the concentration of the AO7 remaining in the solution was determined by UV-Vis absorption spectroscopy (485 nm) based on calibration curves obtained from standard solutions, and the amounts of AO7 adsorbed onto the activated carbons were calculated using $q_e = (C_o - C_e)V/m$, where q_e is the amount of AO7 per gram of adsorbent (mg g⁻¹), V is the volume of the liquid phase (L), C_o is the initial concentration of the solution (mg L⁻¹), C_e is the concentration of the solute in the bulk phase at equilibrium (mg L⁻¹), and m is the amount of adsorbent (g).

2.7. Analysis of the regenerated CAC

CAC samples regenerated under different conditions were dried in air at 378 K for 12 h and used to evaluate the RE. The structural properties and surface chemistry of V-CAC and r-CAC were also investigated.

2.7.1. Evaluation of RE

Regenerated CAC samples were used for the re-adsorption of AO7 (performed under the conditions outlined in section 2.3) to determine the RE (%), which is defined as the ratio of the adsorption capacities of V-CAC and the regenerated CAC, according to $RE = q_r/q_v \times 100\%$, where q_v is the adsorption capacity of V-CAC, that is, the equilibrium amount of contaminant adsorbed per unit mass of V-CAC (mg g⁻¹), and q_r is the adsorption capacity of the regenerated CAC after reaching the re-adsorption equilibrium (mg g⁻¹).

2.7.2. Characterization of structural properties

The structural properties of V-CAC and r-CAC samples were investigated using analysis of their N₂ adsorption isotherms obtained at 77 K using an automatic adsorption system (Autosorb-iQ2-MP, Quantachrome Instruments, USA). Before the experiments, the samples were degassed at 393 K under vacuum for 12.7 h. The micropore area ($S_{\text{micropore}}$), mesoporous area ($S_{\text{mesoporous}}$), total surface area, micropore volume ($V_{\text{micropore}}$), mesoporous volume ($V_{\text{mesoporous}}$), and total pore

volume were obtained according to the non-local density functional theory (NLDFT) equilibrium model.

The morphologies of V-CAC and r-CAC were characterized using scanning electron microscopy (SEM, JEOL S-4800).

2.7.3. Characterization of surface chemistry

The surface chemistries of V-CAC and r-CAC samples were systematically studied. The points of zero charge (PZCs) for V-CAC and r-CAC samples were determined by mass titration [23,24]. The basicities, acidities, and functional groups of V-CAC and r-CAC samples were measured using the titration method of Boehm [25,26].

Fourier-transform infrared spectroscopy (FT-IR, PerkinElmer) was performed using the KBr pellet technique in the range 4,000–400 cm⁻¹ at room temperature to qualitatively identify the functional groups in V-CAC and r-CAC.

3. Results and discussion

3.1. Optimization of the CAC regeneration process

3.1.1. Effect of electrolyte concentration on RE

A series of Na₂SO₄ solutions of different concentrations (pH = 5.2) were used as the electrolyte in regeneration experiments performed at 0.2 A for 6 h with treatment at the cathode. Increasing the Na₂SO₄ concentration from 0.01 to 0.1 M significantly affects RE. This is likely due to an increase in electrolyte conductivity which enables more current to flow and increases the rate of oxidation reactions. However, further increases do not have a positive effect on the RE. The RE remains constant as the concentration is increased from 0.1 to 0.2 M. This may be due to the desorption rate of AO7 controlling the process in this concentration region. The experimental results are shown in Fig. 2. Accordingly, a Na₂SO₄ concentration of 0.1 M was chosen for all subsequent experiments.

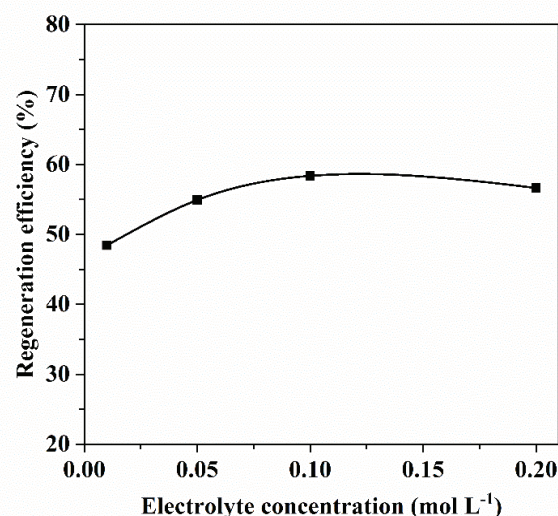


Fig. 2. Effect of Na₂SO₄ concentration on RE. Regeneration conditions: current density 5.71 mA cm⁻²; electrolysis time 6 h; cathode regeneration; electrolyte solution pH 5.2.

3.1.2. Effect of electrolysis time on RE

We examined the effect of electrolysis time on RE. RE initially increases with increasing electrolysis time. The highest RE value of 64% is observed at 6 h, and then it decreases thereafter. The increase in RE is most likely caused by desorption of adsorbed AO7 from the most accessible pores. With time, the desorption of AO7 from the narrow pores becomes difficult because a longer time is required for it to diffuse through the pores. Furthermore, oxidation products, whose adsorption on the activated carbon may also increase with regeneration time, may also block the pore structure of the CAC. Therefore, RE decreases after 6 h. These results are shown in Fig. 3.

3.1.3. Effect of applied current density and electrolysis site (that is, anode or cathode) on RE

The effect of applied current density on RE is illustrated in Fig. 4. When the electrolysis treatment is performed at the cathode, RE increases with increasing current to reach its highest value, almost 79%, at 0.8 A, and then it decreases thereafter. However, for treatment at the anode, the highest RE is achieved at a lower current (0.2 A), and then it decreases slightly with increasing current until a constant value is reached. Fig. 4 also shows that RE values achieved using cathodic regeneration are generally higher than those achieved using anodic regeneration. However, an exception occurs at lower applied currents (0.1 and 0.2 A). At this point, the REs are similar and the anodic treatment shows slightly higher yields. The desorbed AO7 ions are negatively charged at all pH values during our experiments because $pK_{a1} = 1.0$ for the $-SO_3H$ group and $pK_{a2} = 11.4$ for the naphthalene-OH group of AO7 [27,28]. The RE values achieved by cathodic regeneration are generally higher than the corresponding anodic values, and this can be explained in terms of the sign of the polarization of CAC and the electric charge of the adsorbate. For treatment at the cathode, CAC is subjected to a negative potential, which creates a negative

charge on the carbon material. The AO7 ions are also negatively charged. Therefore, AO7 ions desorb more easily from CAC and move farther away by repulsive interactions, leading to a higher RE. Conversely, at the anode, the surface of the CAC is positively charged, inhibiting desorption of the AO7 ions because of electrostatic attraction. Additionally, the applied current has a significant effect on the regeneration process, as higher applied currents increase the extent of polarization, which in turn increases the negative charge accumulating on the CAC particles during cathodic treatment or increases the positive charge accumulating during anodic treatments.

Theoretically, there are two ways to degrade desorbed AO7 ions; anodic electrooxidation or indirect cathodic oxidation by electrogenerated hydrogen peroxide. Hydrogen peroxide is generated by two-electron electroreduction of dissolved oxygen over a wide pH range [29–31], and this process is favored on carbon electrodes [30,32]. Moreover, activated carbon can act as a catalyst for the decomposition of hydrogen peroxide into highly oxidizing hydroxyl radicals [33–35]. During treatment at the cathode, higher applied currents facilitate the desorption of AO7 ions and increase the concentration of oxidizing agents. Therefore, RE increases with increasing current. However, the decrease at higher currents may occur because the adsorption rate of the oxidized products onto CAC is faster than the desorption rate. The highest RE for anodic treatment is achieved at a lower current because it is more difficult for the AO7 ions to desorb at higher applied currents.

3.1.4. Effect of electrolyte pH on RE

Fig. 5 shows the effect of electrolyte pH on RE. RE initially increases as the pH increases and then decreases beyond the maximum value. The pH within an electrochemical cell affects the adsorptive capacity of contaminants, speciation of electrogenerated compounds, the electrosorption/electrodesorption processes, and the rates at which oxidation reactions occur. It is generally understood that high pH values enhance desorption, while low

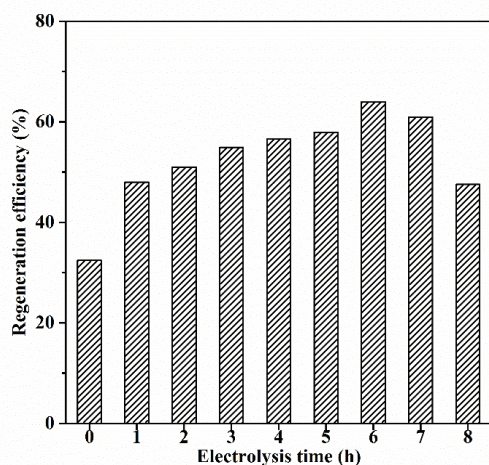


Fig. 3. Effect of electrolysis time on RE. Regeneration conditions: current density 5.71 mA cm^{-2} ; electrolyte concentration $0.1 \text{ M Na}_2\text{SO}_4$; cathode regeneration; electrolyte solution pH 5.2.

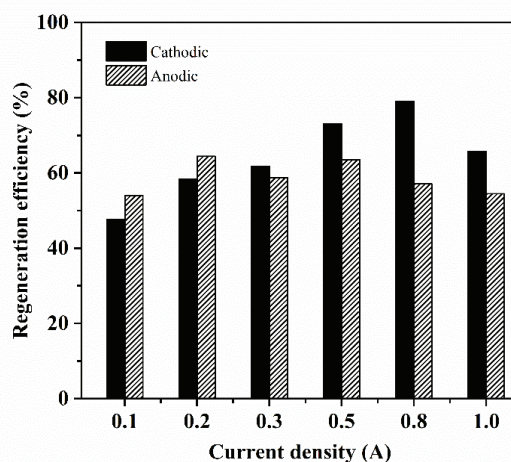


Fig. 4. Effect of applied current and electrolysis treatment on RE. Regeneration conditions: electrolyte concentration $0.1 \text{ M Na}_2\text{SO}_4$; electrolysis time 6 h; electrolyte solution pH 5.2.

pH values enhance oxidation reactions [36]. RE initially increases as pH increases from 1.9 to 11.5, which may be due to either enhanced electrodesorption or the fact that unprotonated species are more easily oxidized than their protonated counterparts [37]. Thereafter, RE decreases as the pH increases from 11.5 to 12.5 because the enhanced desorption is weakened. However, RE does not change very much as the pH increases from 1.9 to 12.5. This is most likely due to protons having an ionic mobility nearly 1.8-times that of hydroxyl ions [38]. Thus, longer operational periods result in an overarching acidic front within the system and decrease the pH of the catholyte if the electrolyte and adsorbent material do not have a large buffering capacity. Consequently, the system pH can be limited as a means to promote the desorption of contaminants and regeneration of exhausted activated carbon.

3.2. Changes in CAC upon electrochemical regeneration

3.2.1. Structural properties and surface chemistry of CAC

To evaluate the effect of electrochemical regeneration on the structural properties of CAC, the porosities and surface areas of V-CAC and r-CAC were compared using the N_2 adsorption method. The data are presented in Table 1, and the pore size distributions are shown in Fig. S1. The decrease in the mesoporous volume of CAC ($0.107 \text{ cm}^3 \text{ g}^{-1}$) is higher than that of the micropore volume ($0.022 \text{ cm}^3 \text{ g}^{-1}$), indicating that the mesopores play a more important role in the

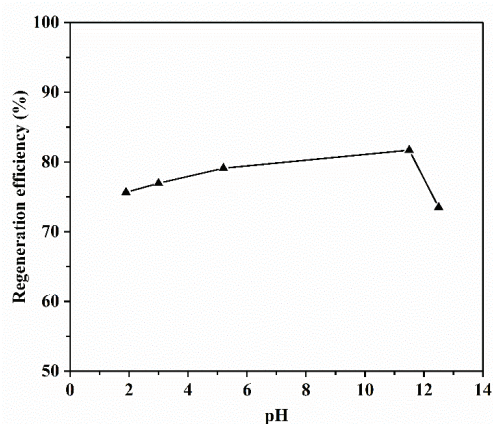


Fig. 5. Effect of electrolyte solution pH on RE. Regeneration conditions: electrolyte concentration $0.1 \text{ M Na}_2\text{SO}_4$; electrolysis time 6 h; current density 22.86 mA cm^{-2} ; cathode regeneration.

Table 1
Structural properties of V-CAC and r-CAC samples

	V-CAC	r-CAC
$S_{\text{micropore}} \text{ m}^2 \text{ g}^{-1}$	1265.900	968.490
$S_{\text{mesoporous}} \text{ m}^2 \text{ g}^{-1}$	411.427	271.859
$S_{\text{DFIT}} \text{ m}^2 \text{ g}^{-1}$	1677.327	1240.349
$V_{\text{micropore}} \text{ cm}^3 \text{ g}^{-1}$	0.404	0.382
$V_{\text{mesoporous}} \text{ cm}^3 \text{ g}^{-1}$	0.436	0.329
$V_{\text{total pore}} \text{ cm}^3 \text{ g}^{-1}$	0.840	0.711

adsorption of AO7 ions. This result is consistent with the findings of Quan et al. [39].

Fig. 6 shows the SEM micrographs of V-CAC and r-CAC. The surface of the CAC is smooth before electrochemical regeneration. However, it becomes rough upon treatment.

We assumed that the surface chemistry of CAC would change after electrochemical regeneration. Table 2 shows the results of acid-base titrations for V-CAC and r-CAC with their pH_{pzc} values in aqueous solutions. V-CAC shows a nearly neutral pH_{pzc} value ($\text{pH}_{\text{pzc}} = 6.894$), that becomes basic ($\text{pH}_{\text{pzc}} = 9.022$) upon regeneration. This is mainly caused by the oxidation of phenolic hydroxyl groups to quinoid carbonyl groups, the removal of carboxyl groups by the alkaline solution, and hydrolysis of lactonic groups under alkaline conditions. Therefore, a decreased number of acidic functional groups and an increased number of basic functional groups are presented by r-CAC.

The surface functional groups on V-CAC and r-CAC were investigated using FTIR, and the spectra are shown in Fig. S2. The results demonstrate that there is no evident difference between V-CAC and r-CAC.

3.2.2. Adsorption kinetics

To investigate the kinetics of AO7 adsorption by V-CAC and r-CAC, three models were evaluated: pseudo-first order, pseudo-second order, and intraparticle diffusion.

The pseudo-first order model can be described according to Namasivayam and Kardivelu [40] by Eq. (1):

$$\log(q_e - q_t) = \log q_e - \frac{k_1}{2.303} t \quad (1)$$

where q_e and q_t are the amounts of the adsorbed adsorbate (mg g^{-1}) at equilibrium and at time, t (h), respectively, and k_1 is the rate constant of adsorption (h^{-1}). The values of k_1 and q_e were calculated from the plots of $\log(q_e - q_t)$ vs t .

The pseudo-second order model [41] is expressed according to Eq. (2):

$$\frac{t}{q_t} = \frac{1}{k_2 q_e^2} + \frac{1}{q_e} t \quad (2)$$

where k_2 ($\text{g mg}^{-1} \text{ h}^{-1}$) is the rate constant for second-order adsorption, and q_e and q_t are the amounts of adsorbed adsorbate (mg g^{-1}) at equilibrium and at time, t (h), respectively. The values of k_2 were obtained from the plot of (t/q_t) vs t .

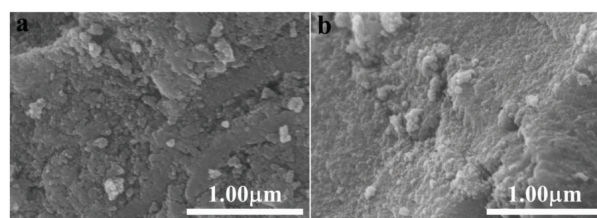


Fig. 6. SEM micrographs of CAC before and after electrochemical regeneration, (a) V-CAC and (b) r-CAC.

The intraparticle diffusion model [42,43] can be described by $q_t = k_p t^{0.5} + C$, where k_p is the intraparticle diffusion constant ($\text{mg g}^{-1} \text{h}^{-0.5}$). The slope of the linear part of the curve (q_t vs $t^{0.5}$) gives the rate of adsorption, which is controlled by intraparticle diffusion. Extrapolating the linear straight lines to the time axis gives the intercepts (C), which are related to the thickness of the boundary layer. In other words, a large

intercept indicates a large boundary layer effect. Therefore, if $C = 0$, the only controlling step is intraparticle diffusion, while if $C \neq 0$, the adsorption process is complex and involves more than one diffusive resistance.

The predicted and experimental q_e values, adsorption rate constants, and correlation coefficients for V-CAC and r-CAC using the three kinetic models were compared. The results are listed in Tables 3–5. For the adsorption of AO7 onto V-CAC, at different temperatures and different initial concentrations, the calculated q_e values agree very well with the experimental data and the correlation coefficients for pseudo-second order kinetic model are higher than those of the pseudo-first order kinetic model and intraparticle diffusion model in all cases. Thus, the adsorption systems follow a pseudo-second order kinetic model, that is, the adsorption reaction controls the adsorption process. However, after electrochemical regeneration, the calculated q_e values for the intraparticle diffusion model are closer to the experimental data than those of the pseudo-first order and pseudo-second order kinetic models. Moreover, the correlation coefficients for the intraparticle diffusion model are higher than 0.99. Therefore, the adsorption of AO7 onto

Table 2
Acid-base properties of V-CAC and r-CAC (mmol g^{-1})

	V-CAC	r-CAC
pH _{pzc}	6.894	9.022
Carboxylic	0.05053	0.02176
Lactonic	0.09504	0.03653
Phenolic	0.4364	0.1974
Basic	0.2865	0.9114
Acidic	0.5820	0.2557
All groups	0.8685	1.1671

Table 3
Kinetic parameters and their correlation coefficients for the adsorption of AO7 onto CAC (Pseudo-first order model)

T/K	Co/ mg L^{-1}	V-CAC (Pseudo-first order)				r-CAC (Pseudo-first order)			
		$k_1/\text{h}^{-1} (\times 10^1)$	$q_{e,\text{exp}}/\text{mg g}^{-1}$	$q_{e,\text{calc}}/\text{mg g}^{-1}$	R^2	$k_1/\text{h}^{-1} (\times 10^1)$	$q_{e,\text{exp}}/\text{mg g}^{-1}$	$q_{e,\text{calc}}/\text{mg g}^{-1}$	R^2
303	100	0.5711	29.305	25.948	0.9835	0.2902	18.359	18.659	0.9897
	300	0.4007	55.275	48.139	0.9832	0.4099	33.945	34.419	0.9740
	500	0.4353	60.993	51.820	0.9910	0.3547	49.979	42.053	0.9695
313	100	0.9857	29.601	26.558	0.9964	0.5021	21.717	25.480	0.9390
	300	0.3270	70.103	56.925	0.9865	0.5573	46.168	55.132	0.8971
	500	0.6679	92.692	103.44	0.8829	0.4882	58.844	62.488	0.8682
323	100	1.7042	29.676	28.236	0.9904	0.4353	22.040	20.749	0.9819
	300	0.4560	82.657	62.835	0.9934	0.4330	50.601	48.719	0.9297
	500	0.4399	98.136	71.367	0.9569	0.4399	69.321	64.372	0.9556

Table 4
Kinetic parameters and their correlation coefficients for the adsorption of AO7 onto CAC (Pseudo-second order model)

T/K	Co/ mg L^{-1}	V-CAC (Pseudo-second order)				r-CAC (Pseudo-second order)			
		$k_2/\text{g mg}^{-1} \text{h}^{-1} (\times 10^2)$	$q_{e,\text{exp}}/\text{mg g}^{-1}$	$q_{e,\text{calc}}/\text{mg g}^{-1}$	R^2	$k_2/\text{g mg}^{-1} \text{h}^{-1} (\times 10^2)$	$q_{e,\text{exp}}/\text{mg g}^{-1}$	$q_{e,\text{calc}}/\text{mg g}^{-1}$	R^2
303	100	0.2738	29.305	33.445	0.9970	0.0579	18.359	30.581	0.9622
	300	0.1039	55.275	63.694	0.9798	0.0869	33.945	44.444	0.9802
	500	0.1021	60.993	70.423	0.9909	0.1212	49.979	55.866	0.9623
313	100	0.5670	29.601	32.258	0.9990	0.0737	21.717	34.014	0.9788
	300	0.0720	70.103	81.301	0.9909	0.0665	46.168	60.606	0.9430
	500	0.0634	92.692	111.11	0.9973	0.0712	58.844	70.922	0.9085
323	100	1.1034	29.676	31.250	0.9992	0.2048	22.040	26.738	0.9867
	300	0.1157	82.657	90.909	0.9926	0.0914	50.601	60.241	0.9669
	500	0.1068	98.136	106.38	0.9902	0.0779	69.321	80.645	0.9688

Table 5
Kinetic parameters and their correlation coefficients for the adsorption of AO7 onto CAC (Intraparticle diffusion model)

T/K	Co/mg L ⁻¹	V-CAC (Intraparticle diffusion)					r-CAC (Intraparticle diffusion)				
		$k_p/\text{mg g}^{-1} \text{h}^{-0.5}$	$q_{e,\text{exp}}/\text{mg g}^{-1}$	$q_{e,\text{calc}}/\text{mg g}^{-1}$	C	R ²	$k_p/\text{mg g}^{-1} \text{h}^{-0.5}$	$q_{e,\text{exp}}/\text{mg g}^{-1}$	$q_{e,\text{calc}}/\text{mg g}^{-1}$	C	R ²
303	100	3.2615	29.305	31.991	4.3163	0.9641	2.4176	18.359	17.575	-2.9387	0.9965
	300	6.2121	55.275	56.803	4.0915	0.9970	4.3154	33.945	34.901	-1.7159	0.9975
	500	6.9682	60.993	64.519	5.3918	0.9768	5.3403	49.979	49.693	4.3789	0.9960
313	100	2.8003	29.601	33.516	9.7545	0.8624	2.9925	21.717	22.887	-2.5052	0.9948
	300	8.0331	70.103	71.166	3.0025	0.9747	5.8990	46.168	48.103	-1.9519	0.9890
	500	10.978	92.692	101.41	8.2538	0.9618	6.7142	58.844	58.955	1.9832	0.9667
323	100	2.1904	29.676	33.337	14.751	0.7724	2.6685	22.040	23.082	0.4386	0.9927
	300	8.3029	82.657	90.217	19.765	0.9825	5.9001	50.601	51.689	1.6245	0.9953
	500	9.3842	98.136	102.48	22.853	0.9756	7.8762	69.321	71.316	4.4842	0.9921

r-CAC obeys the intraparticle diffusion kinetic model, that is, diffusion is the limiting step during the adsorption process. Thus, upon regeneration, the predominant mechanism for the adsorption process changes from reaction-controlled to diffusion-controlled.

3.2.3. Adsorption isotherms

Two common adsorption equilibrium models, that is, the Langmuir and Freundlich models, were used to fit the experimental data for the equilibrium of AO7 adsorption on V-CAC and r-CAC in aqueous solutions at three constant temperatures: 303, 313, and 323 K.

3.2.3.1. Langmuir isotherm Langmuir isotherm theory assumes adsorption on a homogeneous surface [44,45]. The Langmuir equation can be written as shown in Eq. (3):

$$q_e = \frac{Q_m K_L C_e}{1 + K_L C_e}$$

or

$$\frac{C_e}{q_e} = \frac{1}{Q_m K_L} + \frac{C_e}{Q_m}$$

(3)

where C_e is the equilibrium concentration (mg L⁻¹) of AO7, q_e is the amount adsorbed at equilibrium (mg g⁻¹), K_L is the equilibrium adsorption constant related to the affinity of the binding sites (L mg⁻¹), and Q_m is the maximum amount of AO7 per unit weight of adsorbent for complete monolayer coverage (mg g⁻¹).

An essential characteristic of the Langmuir isotherm can be expressed in terms of a dimensionless constant, called the equilibrium parameter (R_L), which is defined according to Eq. (4) [46]:

$$R_L = \frac{1}{1 + (K_L C_0)}$$

(4)

where C_0 is the initial dye concentration (mg L⁻¹). The value of R_L categorizes the isotherm as favourable ($0 < R_L < 1$), linear ($R_L = 1$), unfavorable ($R_L > 1$), or irreversible ($R_L = 0$).

3.2.3.2. Freundlich isotherm The Freundlich isotherm is an empirical equation employed to describe heterogeneous systems [45,47]. It is commonly given by Eq. (5):

$$q_e = K_F C_e^{\frac{1}{n}}$$

or

$$\log q_e = \log K_F + \frac{1}{n} \log C_e$$

(5)

where q_e is the amount of solute adsorbed per unit of adsorbent (mg g⁻¹), C_e is the equilibrium concentration of the solute in the bulk solution (mg L⁻¹), K_F is the Freundlich constant, which is indicative of the relative adsorption capacity of the adsorbent (L^{1/n} g⁻¹ mg^(1-1/n)) and $1/n$ is the adsorption intensity.

The characteristic parameters of the Langmuir and Freundlich isotherm models at several temperatures and the correlation coefficients (R^2) are listed in Table 6. The correlation coefficients (R^2) for V-CAC and r-CAC are higher using the Langmuir isotherm than those using the Freundlich isotherm. Moreover, the dimensionless constant R_L lies within the favorable limit. Therefore, we concluded that the Langmuir isotherm model fits the experimental data better than the Freundlich isotherm model for the adsorption of AO7 onto both V-CAC and r-CAC. However, the calculated values of Q_m for V-CAC are closer to the experimental values than those for r-CAC. This may be explained as follows. Upon electrochemical regeneration, the predominant mechanism for the adsorption process changes from reaction-controlled to diffusion-controlled. The diffusion-controlled mechanism requires more time for r-CAC to reach adsorption saturation. Therefore, during the 72-h adsorption, it did not reach the saturation plateau. Fig. 7 shows the adsorption isotherm for V-CAC, which reaches adsorption saturation after 72-h adsorption. Furthermore, it can be observed that

Table 6
Langmuir and Freundlich isotherm parameters for the adsorption of AO7 onto V-CAC and r-CAC at different temperatures

Adsorbent	T/K	Langmuir isotherm constants				Freundlich isotherm constants		
		$Q_m/\text{mg g}^{-1}$	$K_L/\text{L mg}^{-1}$	R_L	R^2	$K_f/\text{L}^{1/n} \text{g}^{-1} \text{mg}^{(1-1/n)}$	n	R^2
V-CAC	303	65.359	0.0753	0.0259	0.9908	25.757	6.1958	0.9840
	313	92.593	0.0968	0.0202	0.9872	29.744	4.6685	0.9821
	323	101.01	0.2565	0.0077	0.9986	36.358	4.4843	0.9047
r-CAC	303	64.516	0.0087	0.1866	0.9817	3.5091	2.1853	0.9912
	313	72.993	0.0126	0.1366	0.9901	5.5539	2.3855	0.9894
	323	82.645	0.0134	0.1299	0.9674	5.5731	2.2178	0.9341

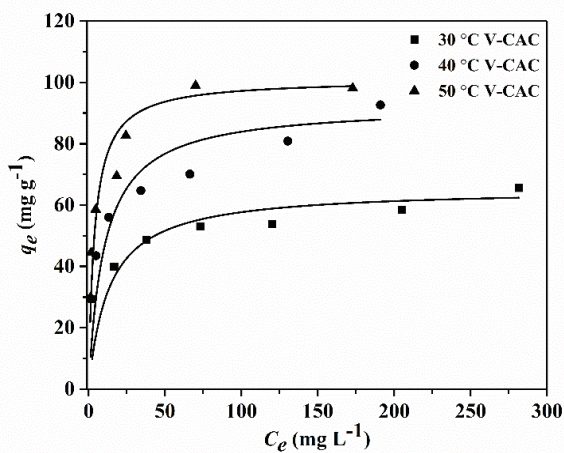


Fig. 7. Effect of temperature on the adsorption of AO7 onto V-CAC.

its adsorption rate is faster than that for r-CAC. Fig. 8 shows the adsorption isotherm for r-CAC. During 72-h adsorption, it does not reach adsorption saturation and the values of Q_m increase when we prolong the adsorption time. Therefore, the experimental data for Q_m are lower than the calculated values.

3.2.4. Adsorption thermodynamic parameters

The thermodynamic parameters that must be considered for determining the type of process are the enthalpy of adsorption (ΔH), entropy change (ΔS), and free energy change (ΔG). The positive value of ΔS suggests an increased randomness at the solid-solution interface during adsorption of the dye in an aqueous solution onto the adsorbents and positive value for ΔH indicates an endothermic process, while a negative value indicates an exothermic process. Another important thermodynamic parameter involved in the adsorption process is ΔG . A negative value of ΔG indicates that the adsorption process decreases the Gibbs free energy, confirming the feasibility of the process and the spontaneous nature of the adsorption with a high preference for AO7 on CAC. The values of ΔS , ΔH , and ΔG were determined from $\ln K_L = \Delta S/R - \Delta H/RT$ and $\Delta G = -RT \ln K_L$ [48], where K_L is the Langmuir constant (L mol^{-1}). T and R are the absolute temperature and universal gas constant, respectively. ΔS and ΔH are calculated from the slope and intercept of the

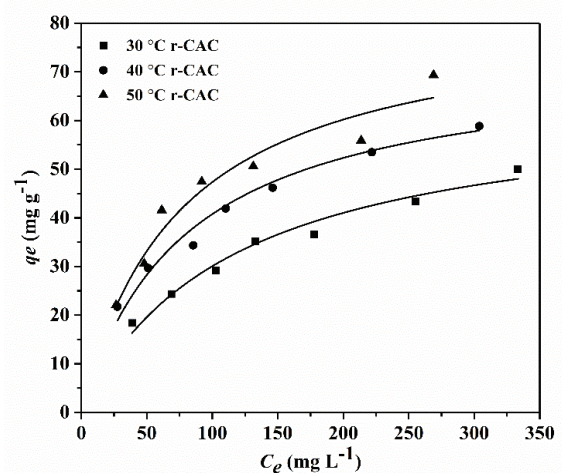


Fig. 8. Effect of temperature on the adsorption of AO7 onto r-CAC.

Table 7
Thermodynamic parameters for adsorption of AO7 onto V-CAC and r-CAC

Adsorbent	T/K	Thermodynamic parameters		
		$\Delta G/\text{kJ mol}^{-1}$	$\Delta H/\text{kJ mol}^{-1}$	$\Delta S/\text{kJ mol}^{-1} \text{K}^{-1}$
V-CAC	303	-25.645	49.702	0.2476
	313	-27.142		
	323	-30.640		
r-CAC	303	-20.212	17.565	0.1251
	313	-21.855		
	323	-22.697		

van't Hoff plots of $\ln K_L$ vs $1/T$. The results are given in Table 7. For V-CAC, the values of ΔG , ΔH , and ΔS are -25.645 to $-30.640 \text{ kJ mol}^{-1}$, $49.702 \text{ kJ mol}^{-1}$, and $0.2476 \text{ kJ mol}^{-1} \text{K}^{-1}$, respectively and for r-CAC, the values of ΔG , ΔH , and ΔS are -20.212 to $-22.697 \text{ kJ mol}^{-1}$, $17.565 \text{ kJ mol}^{-1}$, and $0.1251 \text{ kJ mol}^{-1} \text{K}^{-1}$, respectively. Both adsorbents present a positive value of ΔS (which suggests an increased randomness), a positive value of ΔH (which indicates an endothermic process), and a negative value of ΔG (which indicates the feasibility of the process and the spontaneous nature of the adsorption). Moreover,

compared with those for V-CAC, the absolute values of ΔG , ΔH , and ΔS are smaller for r-CAC, which reveals that after electrochemical regeneration, the adsorption rate and the adsorption capacity of CAC decrease substantially.

4. Conclusion

In this study, we developed and optimized a regeneration process for activated carbon. The best result in terms of RE was obtained by cathodic regeneration in a 0.1 M Na_2SO_4 electrolyte (pH = 11.5) at a constant current of 0.8 A and a regeneration time of 6 h. Under these conditions, a slightly higher RE (>80%) is achieved. The structural properties and surface chemistries of V-CAC and r-CAC were investigated, revealing that many residual AO7 and oxidation species remain adsorbed on the activated carbon, decreasing its adsorption capacity. Moreover, fewer acidic functional groups and more basic functional groups are present on r-CAC. The adsorption kinetics, adsorption equilibrium isotherms, and adsorption thermodynamic parameters for V-CAC and r-CAC were systematically evaluated. The adsorption system follows a pseudo-second-order kinetic model for V-CAC. However, after regeneration, the adsorption system obeys an intraparticle diffusion kinetic model revealing that the predominant mechanism for the adsorption process is converted from a reaction-controlled mechanism to a diffusion-controlled mechanism upon regeneration. The adsorption equilibrium isotherms were analyzed using the Langmuir and Freundlich isotherm equations. The adsorption data fit well with the Langmuir model for both V-CAC and r-CAC. The thermodynamic parameters ΔS , ΔH , and $-\Delta G$ for V-CAC and r-CAC are positive, revealing that the adsorption process is endothermic and spontaneous. However, the absolute values of ΔG , ΔH , and ΔS are lower for r-CAC than for V-CAC, indicating that the adsorption rate and the adsorption capacity of CAC significantly decreased upon electrochemical regeneration. The concentration of AO7 in the electrolyte was very low so that we could not detect it using UV-Vis spectra after electrochemical treatment. More work is required to investigate the mechanism of organic-molecule breakdown and to identify the oxidation products that form during electrochemical regeneration.

Acknowledgments

This research did not receive any special grant from funding agencies in the public, commercial, or not-for-profit sectors.

Declarations of interest: None

References

- [1] G. Crini, Non-conventional low-cost adsorbents for dye removal: a review, *Bioresour. Technol.*, 97 (2006) 1061–1085.
- [2] F.M. Mohammed, E.P.L. Roberts, A. Hill, A.K. Campen, N.W. Brown, Continuous water treatment by adsorption and electrochemical regeneration, *Water Res.*, 45 (2011) 3065–3074.
- [3] V.K. Gupta, I. Ali, V.K. Saini, Adsorption studies on the removal of Vertigo Blue 49 and Orange DNA13 from aqueous solutions using carbon slurry developed from a waste material, *J. Colloid Interface Sci.*, 315 (2007) 87–93.
- [4] A.M. Aljeboree, A.N. Alshirifi, A.F. Alkaim, Kinetics and equilibrium study for the adsorption of textile dyes on coconut shell activated carbon, *Arabian J. Chem.*, 10 (2017) S3381–S3393.
- [5] C.H. Weng, M.C. Hsu, Regeneration of granular activated carbon by an electrochemical process, *Sep. Purif. Technol.*, 64 (2008) 227–236.
- [6] S. Lopez-Bernabeu, R. Ruiz-Rosas, C. Quijada, F. Montilla, E. Morallon, Enhanced removal of 8-quinolinecarboxylic acid in an activated carbon cloth by electroadsorption in aqueous solution, *Chemosphere*, 144 (2016) 982–988.
- [7] N.W. Brown, E.P.L. Roberts, A.A. Garforth, R.A.W. Dryfe, Electrochemical regeneration of a carbon-based adsorbent loaded with crystal violet dye, *Electrochim. Acta*, 49 (2004) 3269–3281.
- [8] R. Berenguer, J.P. Marco-Lozar, C. Quijada, D. Cazorla-Amoros, E. Morallon, Electrochemical regeneration and porosity recovery of phenol-saturated granular activated carbon in an alkaline medium, *Carbon*, 48 (2010) 2734–2745.
- [9] A. Ahmad, S.H. Mohd-Setapar, C.S. Chuong, A. Khatoun, W.A. Wani, R. Kumar, M. Rafatullah, Recent advances in new generation dye removal technologies: novel search for approaches to reprocess wastewater, *RSC Adv.*, 5 (2015) 30801–30818.
- [10] Y.H. Han, X. Quan, X.L. Ruan, W.D. Zhang, Integrated electrochemically enhanced adsorption with electrochemical regeneration for removal of acid orange 7 using activated carbon fibers, *Sep. Purif. Technol.*, 59 (2008) 43–49.
- [11] R. Berenguer, J.P. Marco-Lozar, C. Quijada, D. Cazorla-Amoros, E. Morallon, Comparison among chemical, thermal, and electrochemical regeneration of phenol-saturated activated carbon, *Energy Fuel*, 24 (2010) 3366–3372.
- [12] T.L. Zheng, Q.H. Wang, Z.N. Shi, Z.H. Zhang, Y.H. Ma, Microwave regeneration of spent activated carbon for the treatment of ester-containing wastewater, *RSC Adv.*, 6 (2016) 60815–60825.
- [13] G.S. Miguel, S.D. Lambert, N.J. Graham, The regeneration of field-spent granular-activated carbons, *Water Res.*, 35 (2001) 2740–2748.
- [14] R.M. Narbaitz, J. McEwen, Electrochemical regeneration of field spent GAC from two water treatment plants, *Water Res.*, 46 (2012) 4852–4860.
- [15] B. Karabacakoglu, O. Savlak, Electrochemical regeneration of Cr (VI) saturated granular and powder activated carbon: Comparison of regeneration efficiency, *Ind. Eng. Chem. Res.*, 53 (2014) 13171–13179.
- [16] Y.H. Han, X. Quan, S. Chen, H.M. Zhao, C.Y. Cui, Y.Z. Zhao, Electrochemically enhanced adsorption of aniline on activated carbon fibers, *Sep. Purif. Technol.*, 50 (2006) 365–372.
- [17] O. Zanella, D. Bilibio, W.L. Priamo, I.C. Tessaro, L.A. Feris, Electrochemical regeneration of phenol-saturated activated carbon-proposal of a reactor, *Environ. Technol.*, 38 (2017) 549–557.
- [18] T. Velegraki, I. Poullos, M. Charalabaki, N. Kalogerakis, P. Samaras, D. Mantzavinos, Photocatalytic and sonolytic oxidation of acid orange 7 in aqueous solution, *Appl. Catal. B-Environ.*, 62 (2006) 159–168.
- [19] C. Cai, H. Zhang, X. Zhong, L.W. Hou, Ultrasound enhanced heterogeneous activation of peroxydisulfate by a bimetallic Fe-Co/SBA-15 catalyst for the degradation of Orange II in water, *J. Hazard. Mater.*, 283 (2015) 70–79.
- [20] L.C. Davies, I.S. Pedro, J.M. Novais, S. Martins-dias, Aerobic degradation of acid orange 7 in a vertical-flow constructed wetland, *Water Res.*, 40 (2006) 2055–2063.
- [21] C. Guillard, H. Lachheb, A. Houas, M. Ksibi, E. Elaloui, J.M. Herrmann, Influence of chemical structure of dyes, of pH and of inorganic salts on their photocatalytic degradation by TiO₂ comparison of the efficiency of powder and supported TiO₂, *J. Photochem. Photobiol. A*, 158 (2003) 27–36.
- [22] T. Hirakawa, Y. Nosaka, Properties of O₂⁻ and ·OH formed in TiO₂ aqueous suspensions by photocatalytic reaction and the influence of H₂O₂ and some ions, *Langmuir*, 18 (2002) 3247–3254.

- [23] S.S. Barton, M.J.B. Evans, E. Halliop, J.A.F. MacDonald, Acidic and basic sites on the surface of porous carbon, *Carbon*, 35 (1997) 1361–1366.
- [24] J.S. Noh, J.A. Schwarz, Effect of HNO₃ treatment on the surface acidity of activated carbons, *Carbon*, 28 (1990) 675–682.
- [25] Y.Y. Xue, G.Z. Lu, Y. Guo, Y.L. Guo, Y.Q. Wang, Z.G. Zhang, Effect of pretreatment method of activated carbon on the catalytic reduction of NO by carbon over CuO, *Appl. Catal. B-Environ.*, 79 (2008) 262–269.
- [26] H.P. Boehm, Surface oxides on carbon and their analysis: a critical assessment, *Carbon*, 40 (2002) 145–149.
- [27] W.L. Chou, C.T. Wang, C.P. Chang, Comparison of removal of acid orange 7 by electrooxidation using various anode materials, *Desalination*, 266 (2011) 201–207.
- [28] F. Herrera, A. Lopez, G. Mascolo, E. Albers, J. Kiwi, Catalytic combustion of orange II on hematite: surface species responsible for the dye degradation, *Appl. Catal. B-Environ.*, 29 (2001) 147–162.
- [29] Y.L. Hsiao, K. Nobe, Hydroxylation of chlorobenzene and phenol in a packed bed flow reactor with electrogenerated Fenton's reagent, *J. Appl. Electrochem.*, 23 (1993) 943–946.
- [30] A. Alvarez-Gallegos, D. Pletcher, The removal of low level organics via hydrogen peroxide formed in a reticulated vitreous carbon cathode cell, Part 1. The electroynthesis of hydrogen peroxide in aqueous acidic solutions, *Electrochim. Acta*, 44 (1998) 853–861.
- [31] R. Berenguer, J.P. Marco-Lozar, C. Quijada, D. Cazorla-Amoros, E. Morallon, Effect of electrochemical treatments on the surface chemistry of activated carbon, *Carbon*, 47 (2009) 1018–1027.
- [32] Z.M. Qiang, J.H. Chang, C.P. Huang, Electrochemical generation of hydrogen peroxide from dissolved oxygen in acidic solutions, *Water Res.*, 36 (2002) 85–94.
- [33] H.H. Huang, M.C. Lu, J.N. Chen, C.T. Lee, Catalytic decomposition of hydrogen peroxide and 4-chlorophenol in the presence of modified activated carbons, *Chemosphere*, 51 (2003) 935–943.
- [34] F. Lucking, H. Koser, M. Jank, A. Ritter, Iron powder, graphite and activated carbon as catalysts for the oxidation of 4-chlorophenol with hydrogen peroxide in aqueous solution, *Water Res.*, 32 (1998) 2607–2614.
- [35] M.H. Zhou, L.C. Lei, The role of activated carbon on the removal of p-nitrophenol in an integrated three-phase electrochemical reactor, *Chemosphere*, 65 (2006) 1197–1203.
- [36] R.V. Mcquillan, G.W. Stevens, K.A. Mumford, The electrochemical regeneration of granular activated carbons: A review, *J. Hazard. Mater.*, 355 (2018) 34–49.
- [37] C.A. Martínez-Huitle, M.A. Rodrigo, I. Sirés, O. Scialdone, Single and coupled electrochemical processes and reactors for the abatement of organic Water pollutants: a critical review, *Chem. Rev.*, 115 (2015) 13362–13407.
- [38] Y.B. Acar, A.N. Alshawabkeh, Principles of electrokinetic remediation, *Environ. Sci. Technol.*, 27 (1993) 2638–2647.
- [39] X. Quan, X.T. Liu, L.L. Bo, S. Chen, Y.Z. Zhao, X.Y. Cui, Regeneration of acid orange 7-exhausted granular activated carbons with microwave irradiation, *Water Res.*, 38 (2004) 4484–4490.
- [40] C. Namasivayam, K. Kadirvelu, Uptake of mercury (II) from wastewater by activated carbon from an unwanted agricultural solid by-product: coirpith, *Carbon*, 37 (1999) 79–84.
- [41] F. Nekouei, S. Nekouei, I. Tyagi, V.K. Gupta, Kinetic, thermodynamic and isotherm studies for acid blue 129 removal from liquids using copper oxide nanoparticle-modified activated carbon as a novel adsorbent, *J. Mol. Liq.*, 201 (2015) 124–133.
- [42] N. Thinakaran, P. Baskaralingam, K.V.T. Ravi, P. Panneerselvam, Adsorptive removal of acid blue 15: equilibrium and kinetic study, *Clean-Soil Air Water*, 36 (2008) 798–804.
- [43] G. McKay, V.J.P. Poots, Kinetics and diffusion processes in colour removal from effluent using wood as an adsorbent, *J. Chem. Technol. Biotechnol.*, 30 (1980) 279–292.
- [44] I. Langmuir, The adsorption of gases on plane surfaces of glass, mica and platinum, *J. Am. Chem. Soc.*, 40 (1918) 1361–1403.
- [45] P. Hadi, M. Xu, C. Ning, C.S.K. Lin, G. McKay, A critical review on preparation, characterization and utilization of sludge-derived activated carbons for wastewater treatment, *Chem. Eng. J.*, 260 (2015) 895–906.
- [46] M. Khan, I.M.C. Lo, Removal of ionizable aromatic pollutants from contaminated water using nano γ -Fe₂O₃ based magnetic cationic hydrogel: Sorptive performance, magnetic separation and reusability, *J. Hazard. Mater.*, 322 (2017) 195–204.
- [47] M.E. Fernandez, B. Ledesma, S. Roman, P.R. Bonelli, A.L. Cukierman, Development and characterization of activated hydrochars from orange peels as potential adsorbents for emerging organic contaminants, *Bioresource Technol.*, 183 (2015) 221–228.
- [48] A. Rodríguez, J. García, G. Ovejero, M. Mestanza, Adsorption of anionic and cationic dyes on activated carbon from aqueous solutions: equilibrium and kinetics, *J. Hazard. Mater.*, 172 (2009) 1311–1320.

Supplementary information

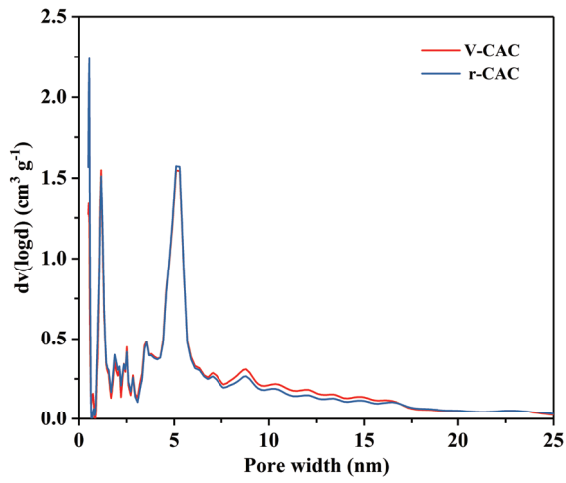


Fig. S1. Pore size distributions of V-CAC and r-CAC determined using the NLDFT method.

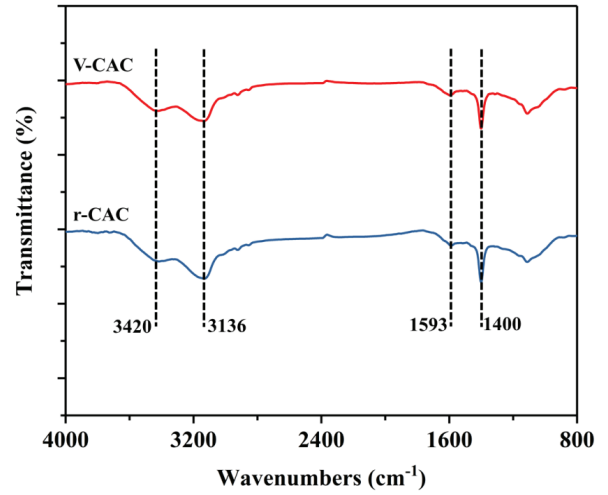


Fig. S2. FTIR spectra of V-CAC and r-CAC.